

LARGE-SCALE STRUCTURE OF EMISSION-LINE GALAXIES AT $z = 3.1^1$

TOMOKI HAYASHINO,² YUICHI MATSUDA,^{2,3} HAJIME TAMURA,² RYOSUKE YAMAUCHI,² TORU YAMADA,³ MASARU AJIKI,⁴ SHINOBU S. FUJITA,⁴ TAKASHI MURAYAMA,⁴ TOHRU NAGAO,⁴ KOUJI OHTA,⁵ SADANORI OKAMURA,^{6,7} MASAMI OUCHI,⁶ KAZUHIRO SHIMASAKU,^{6,7} YASUHIRO SHIOYA,⁴ AND YOSHIAKI TANIGUCHI⁴

Received 2004 January 2; accepted 2004 August 4

ABSTRACT

We obtained a deep wide-field ($32' \times 24'$) narrowband ($\lambda_c = 4977\text{\AA}$, $\Delta\lambda = 77\text{\AA}$) image of a field including the protocluster at $z = 3.1$ in the SSA22a field studied by Steidel et al. using the Subaru Telescope. The field we observed is about 10 times as large as that studied by Steidel et al. We detected 283 highly confident strong Ly α emitter candidates at $z \sim 3.1$ down to 25.8 AB mag with the observed equivalent width larger than 154 Å. These strong Ly α emitter candidates show a highly nonuniform distribution with the beltlike region of high surface density, which is found to extend over ~ 60 Mpc in comoving scale. The average number density of the strong Ly α emitter candidates in this high-density region is 3 times as high as that of a blank field. The probability of finding such a large-scale high-density peak is as small as 0.1% in the context of the CDM structure formation scenario, if we assume a linear bias parameter $b \sim 4$. In addition to these strong Ly α emitters, we also detected 49 Ly α absorbers, which show significant deficit in the narrowband image. We further detected 74 extended emitters, which have significant fluxes over the areas of 18 arcsec 2 or more. Interestingly, both these absorbers and extended emitters show sky distributions very similar to that of the strong Ly α emitters. This supports the reality of the large-scale structure at $z = 3.1$ and suggests that galaxy formation preferentially occurs in the high-density region of strong Ly α emitters.

Key words: cosmology: observations — galaxies: high-redshift — galaxies: photometry — large-scale structure of universe

1. INTRODUCTION

Star-forming galaxies at $z > 3$ show strong spatial clustering at large scales, sometimes over a few tens of megaparsecs in comoving length (Steidel et al. 1998; Adelberger et al. 1998; Ouchi et al. 2001, 2003; Shimasaku et al. 2003). Since mass fluctuation at such large scales is expected to be very small at high redshift in the cold dark matter (CDM)-dominated universe, the distribution of star-forming galaxies is considered to be strongly biased to mass (e.g., Governato et al. 1998; Kauffmann et al. 1999; Cen & Ostriker 2000). A large-bias parameter value, $b = 4\text{--}8$, where $\sigma_{\text{LBG}} = b\sigma_{\text{mass}}$, is needed to naturally explain the observational results (Steidel et al. 1998; Adelberger et al. 1998). The strong density peaks of the CDM at such high redshifts may correspond to protoclusters in which the early galaxy formation proceeds (Governato et al. 1998).

The galaxy concentration at $z = 3.1$ in the SSA22a field (Steidel et al. 1998) is one of the most conspicuous high-density regions of star-forming galaxies known so far. Steidel et al. (1998) first discovered that there is a strong redshift spike of Lyman break galaxies (LBGs) in this field whose

overdensity is the highest among all the regions they studied (Steidel et al. 1998; Adelberger et al. 1998). The density enhancement of those LBGs in the area of $8.7' \times 8.9'$ amounts to 6.0 ± 1.2 (Steidel et al. 2000). In their follow-on narrowband imaging, Steidel et al. (2000) also detected 72 Ly α emitters at $z = 3.054\text{--}3.120$, with observed equivalent width larger than 80 Å in the SSA22a field down to $m_{\text{AB}} = 25.0$, and showed that the surface density of Ly α emitters is also 6 times as large as that in other fields. They also discovered two spectacular objects in this region, namely the gigantic “Ly α blobs” (LABs) whose nature is still not fully understood (Steidel et al. 2000; Chapman et al. 2001; Ohyama et al. 2003).

In spite of progress in studying internal structures of the galaxy density peak at $z = 3.1$ in the SSA22a, the true spatial extent of the high-density region has not been revealed so far, while the physical dimension is essential in understanding the nature of the density peak. It is likely that the true angular extension of the region is larger than $8.7' \times 8.9'$, since the Ly α emitters detected in Steidel et al. (2000) seem to be distributed rather uniformly over their observed area. We therefore conduct further wide-area and deep narrowband imaging of the field, including the SSA22a peak. Using the Subaru 8.2 m telescope equipped with Suprime-Cam, we are able to observe the area about 10 times as large as that studied in Steidel et al. (2000) to investigate the sky distribution of Ly α emitters. If the high-density region of Ly α emitters is a place where galaxies are preferentially formed, it is also important to reveal general properties of the objects there. Then we search not only for strong emitters but also for more diffuse emitters, as well as for Ly α absorption-line objects in the field. In this paper we present our findings regarding these objects and show their overall sky distributions. Further detailed properties of the objects will be reported in the future. We describe our observations and data reduction in § 2 and present the obtained

¹ Based on data collected at Subaru Telescope, which is operated by the National Astronomical Observatory of Japan.

² Neutrino Center, Graduate School of Science, Tohoku University, Aramaki, Aoba, Sendai 980-8578, Japan.

³ National Astronomical Observatory, Mitaka, Tokyo 181-8588, Japan.

⁴ Astronomical Institute, Graduate School of Science, Tohoku University, Aramaki, Aoba, Sendai 980-8578, Japan.

⁵ Department of Astronomy, Graduate School of Science, Kyoto University, Kitashirakawa, Sakyo, Kyoto 606-8502, Japan.

⁶ Department of Astronomy, School of Science, University of Tokyo, Tokyo 113-0033, Japan.

⁷ Research Center for the Early Universe, School of Science, University of Tokyo, Tokyo 113-0033, Japan.

spatial distribution of the Ly α emitters and absorbers in § 3. We give our conclusions and discussion in § 4. Throughout the paper, we adopt the totally flat cosmology, with $\Omega_M = 0.3$, $\Omega_\Lambda = 0.7$, and $H_0 = 70 h_{70} \text{ km s}^{-1} \text{ Mpc}^{-1}$.

2. OBSERVATIONS AND DATA REDUCTION

On 2002 September 8 and 9 (UT), we observed a field centered on the coordinate $(\alpha, \delta) = (22^{\text{h}}17^{\text{m}}.6, +00^\circ17')$ with Suprime-Cam (Miyazaki et al. 2002), using the narrowband filter NB497 with the central wavelength of 4977 Å and the bandwidth of 77 Å, together with the B , V , and R filters, in order to detect Ly α emission- and absorption-line objects at $z = 3.061$ –3.125. The center of the SSA22a region studied by Steidel et al. (2000) lies 2' south of the center of our field. To supplement our own images, we also used the images of the same field from the Subaru data archive taken in R (1.3 hr), i' (1.6 hr), and z' bands (1.1 hr) (2000 August and 2001 October, PI: E. Hu). The net integration times are 1.2, 1.8, 2.9, 1.6, 1.1, and 7.2 hr in total for the B , V , R , i' , z' , and NB497 bands, respectively. The data were reduced using IRAF and the mosaic-CCD data reduction software developed by Yagi et al. (2002). The combined images in the six bands were aligned and smoothed with Gaussian kernels to match their seeing sizes. The average stellar profile of the final images has a FWHM of 1''.0. All the data were calibrated using the standard stars, SA95-42 and LDS749B. The magnitude and color values used here are all measured in the AB system. We corrected for a Galactic reddening value of $E(B - V) = 0.08$ (Steidel et al. 2000), which amounts to 0.3 mag for NB497. The limiting magnitudes for galaxies after the correction are $B_{AB} = 26.5$, $V_{AB} = 26.6$, $R_{AB} = 26.7$, $i'_{AB} = 26.4$, $z'_{AB} = 25.7$, and $NB497 = 26.2$, for 5 σ in a 2'' diameter aperture. From the B - and V -band images, we also constructed the “ BV ” image by combining them as $(2B + V)/3$, so that its effective central wavelength is matched to that of the narrowband filter. Object detection and photometry were performed by using SExtractor version 2.1.6 (Bertin & Arnouts 1996). We adopted “5 connected pixels above 2 σ ” as our detection criterion in making the two source catalogs selected on the NB497 and the BV images. They are used in searching for emitters (§ 3.1) and absorbers (§ 3.2). In the present analysis, magnitudes and colors are measured with a 2'' diameter aperture, except for the extended emitters (§ 3.3). We further limit our NB497 source catalog to $NB497 < 25.8$ ($S/N > 7.5$) and the BV source catalog to $BV < 26.2$ ($S/N > 8$) to avoid noise contamination at a very high confidence level. The total size of the field is 31.7' by 24.3', which corresponds to comoving transverse dimensions of $59.3 h_{70}^{-1} \times 45.5 h_{70}^{-1} \text{ Mpc}$ at $z = 3.1$. The total solid angle used in this paper is 699 arcmin² after removing masked areas where bright stars disturb the correct photometry. The half-power width of NB497 corresponds to a comoving depth of 59.0 h_{70}^{-1} Mpc along the line of sight. The effective comoving volume covered by the NB497 image is thus 144,000 h_{70}^{-3} Mpc³. Note that this is about 10 times as large as the previous narrowband survey in this field by Steidel et al. (2000), 16,500 h_{70}^{-3} Mpc³. The limiting magnitude of our NB497 image is also 0.4 mag deeper than that of Steidel et al. (2000).

As a control sample, a relatively shallow NB497 image of a blank field centered at $(\alpha, \delta) = (02^{\text{h}}18^{\text{m}}, -05^\circ12')$ in the Subaru-XMM Deep Survey Field (Watson & Sekiguchi 2001) is obtained during the same nights, allowing us to compare the surface number density of Ly α emitters with that in our SSA22 field. The control field, hereafter referred to as the SXDS-GT field, is the same field as that observed in Ouchi et al. (2001).

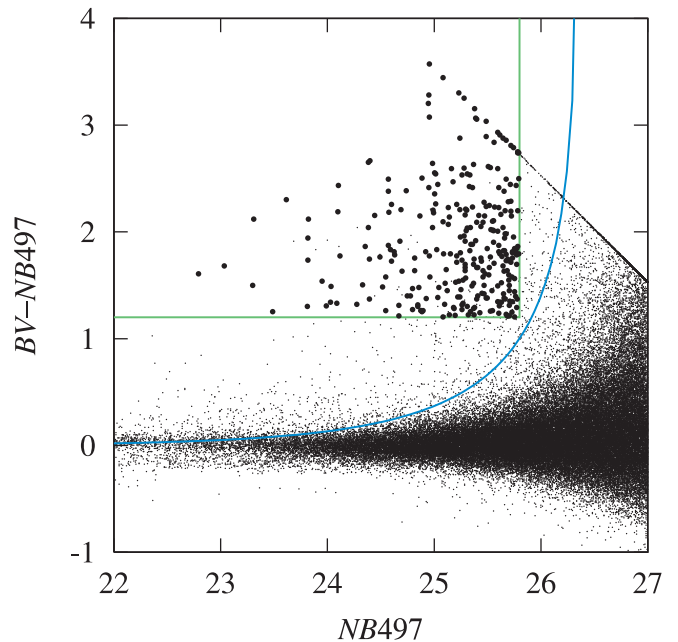


FIG. 1.—Color-magnitude plot for the NB497 selected objects. The blue line indicates the 4 σ confidence level for NB497 excess emission. The horizontal green line shows $BV - NB497 = 1.2$, i.e., $EW_{\text{obs}} = 154 \text{ \AA}$ and the vertical green line indicates $NB497 = 25.8$ ($S/N = 7.5$) after correction for the Galactic extinction (see text). The strong Ly α emitter candidates at $z = 3.1$ that satisfy the criteria presented in the text are indicated by large filled circles.

The broadband images taken by Ouchi et al. (2001) are also used in this paper. The SXDS-GT field data were reduced and analyzed in the same manner as the SSA22 data. The 7 σ detection limit for NB497 image of the SXDS-GT field is 25.3 mag.

3. CANDIDATE Ly α OBJECTS AND A SKY MAP

3.1. Strong Emitters

In Figure 1 we show a color-magnitude diagram for the NB497-selected objects. To pick up $z = 3.1$ strong Ly α emitters, we apply the following criteria: (1) $NB497 < 25.8$ ($S/N > 7.5$) and (2) $BV - NB497 > 1.2$, which correspond to the observed equivalent width (EW) limit of $EW_{\text{obs}} > 154 \text{ \AA}$ or the rest-frame limit of $EW_0 > 40 \text{ \AA}$ for Ly α at $z = 3.1$. Criteria 2 is set to reject [O II] $\lambda 3727$ emitters at $z = 0.33$ with high confidence. Most of the observed [O II] emission-line galaxies at $z < 0.5$ have EW_0 smaller than 50 Å, and those with $EW_0 > 100 \text{ \AA}$ are very rare (e.g., Hammer et al. 1997; Treyer et al. 1998; Sullivan et al. 2000). In addition, we apply one of the following two criteria: (3) $B_{AB} - V_{c,AB} > 0.2$ for the objects with $V_c < 26.9$ ($S/N > 4$), for which $B_{AB} - V_{c,AB}$ color can be measured with reasonable accuracies; or (4) $BV - NB497 > 1.5$ ($EW_{\text{obs}} > 267 \text{ \AA}$) for the fainter objects with $V_{c,AB} > 26.9$, to avoid contamination by strong Mg II $\lambda 2800$ /C III] $\lambda 1909$ /C IV $\lambda 1550$ objects at lower redshifts. Here, $V_{c,AB}$ represents the emission-line free V -band magnitude obtained after subtracting the narrowband flux from the V -band flux. Note that Ly α galaxies at $z \sim 3$, which often have continuum spectra $f_\nu \sim \nu^0$, should have $B_{AB} - V_{c,AB} > 0.2$ because of continuum depression $D_A \sim 0.3$ (Madau 1995), while active galaxies having very strong emission lines at lower redshifts must exhibit bluer continua with $B_{AB} - V_{AB} < 0$. Out of 321 objects that passed criteria 1 and 2, 23 and 15

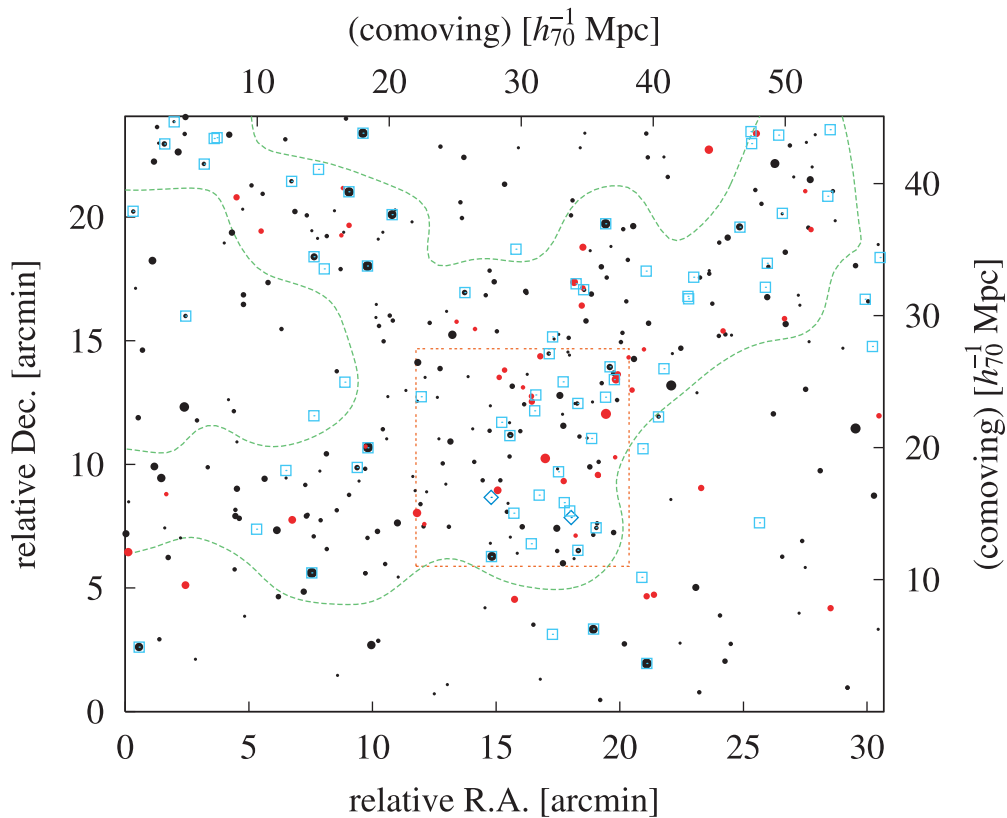


FIG. 2.—Sky distribution of the 283 strong Ly α emitters of the SN7.5 sample (black filled circles), the Ly α absorbers (red filled circles), and the extended Ly α emitters (blue open squares). East is to the left, and north is upward. The sizes of the symbols for the emitters and the absorbers are proportional to the NB flux and the BV flux, respectively. Two LABs found by Steidel et al. are shown with blue open diamonds. The green dashed lines indicate the high-density region of the strong Ly α emitters of the SN7.5 sample (see text). The SSA22a region investigated by Steidel et al. is represented by the orange dotted line.

objects were removed by the additional criteria 3 and 4, respectively. The criteria adopted are so strict that contamination by fake emitters is considered to be very small. Only 0.01 non-NB-excess objects (i.e., $BV - NB497 \approx 0$) are expected to be contaminating our emitter sample due to photometric errors.

The total of 283 highly confident candidates of strong Ly α emitters (LAEs) selected in this way, which are referred to as the SN7.5 sample, are distributed in the Suprime-Cam field as shown in Figure 2 (filled black circles). The two gigantic blobs (Steidel et al. 2000) were detected with our criteria as concentrations of several separated LAEs, and we have tentatively removed these LAEs from the current sample. The SSA22a area studied in Steidel et al. (2000) is indicated by the orange dotted line in Figure 2. The green dashed lines represent the contour where the local number density of the LAEs after smoothing with a Gaussian kernel with $\sigma = 1.5'$ is equal to the

mean value of the entire field. We see a beltlike large structure of the LAEs of 60 Mpc long and 15–20 Mpc wide in comoving scale running from the northwest to the southeast, together with a rather orthogonal structure 30 Mpc long and 15 Mpc wide extending from the field center to the northeast. On the other hand, the southern part of the field seems to be a low-density region of the LAEs. We hereafter refer to the area surrounded by the green dashed lines as “the high-density region” (HDR) of LAEs. The numbers of the LAEs in the HDR and in the entire field are summarized in Table 1. Steidel et al. (2000) detected 77 emission-line objects (five were classified as foreground objects) brighter than $m_{NB} < 25.0$ and with EW larger than 80 Å in the 77.4 arcmin 2 area. For comparison, we also applied the same criteria as theirs and detected 83 objects in the same area. The numbers show good agreement, if we consider photometric errors. We also applied criteria 2 and 3 to

TABLE 1
NUMBER OF LY α EMITTERS, ABSORBERS, AND EXTENDED LY α EMITTERS DETECTED IN THE SSA22 AND THE SXDS-GT FIELDS

Region	Area (arcmin 2)	N_{em}^{a} $\text{NB497} < 25.8$	$N_{\text{abs}}^{\text{b}}$ $BV < 26.2$	N_{em}^{c}	N_{em}^{d} $\text{NB497} < 25.3$	Number Density (arcmin $^{-2}$)	Ratio
SSA22 all.....	699	283	49	74	109	0.16	1.7
SSA22 HDR	302	205	41	56	77	0.26	2.8
SXDF-GT.....	606	55	0.091	1

^a Number of Ly α emitters with $\text{NB497} < 25.8$.

^b Number of Ly α absorbers with $BV < 26.2$.

^c Number of extended Ly α emitters.

^d Number of Ly α emitters with $\text{NB497} < 25.3$.

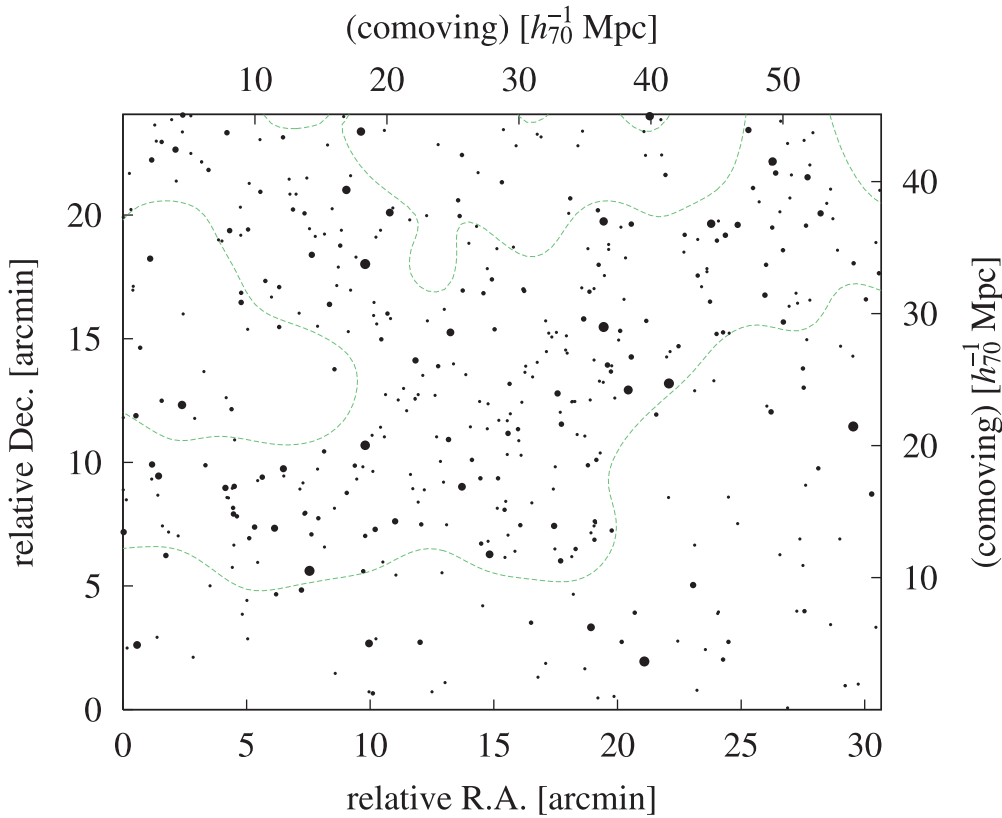


FIG. 3.—Sky distribution of the 424 Ly α emitters with the lower flux and EW limits presented in the text (black filled circles). The sizes of the symbols are proportional to the NB flux. The green dashed lines indicate the high-density region of the emitters, determined similarly as in Fig. 2.

the data of the SXDS-GT field to detect 55 LAEs brighter than $\text{NB497} = 25.3$ in the area of 606 arcmin 2 . The numbers of LAEs in our SSA22 field with the same NB497 limit are 109 and 77 in the entire field and the HDR, with areas of 699 and 302 arcmin 2 , respectively (Table 1). The surface densities of these LAEs in our entire SSA22 field, the HDR, and the SXDF-GT are 0.16, 0.26, and 0.091 arcmin $^{-2}$, respectively.

We also examine the robustness of the shape of the HDR by applying different criteria in our emitter selection. Figure 3 shows the sky map of the 424 emitters that are selected by the criteria with lower limiting flux and EW, (1') $\text{NB497} < 26.0$ ($S/N > 6.0$) and (2') $BV - \text{NB497} > 1.0$ ($\text{EW}_{\text{obs}} > 116 \text{ \AA}$ or $\text{EW}_0 > 28 \text{ \AA}$ for Ly α at $z = 3.1$), where the other criteria are the same as those for the SN7.5 sample. In Figure 3, the high-density region defined in the same manner as that for the SN7.5 sample is indicated by green dashed lines. We confirmed that the overall shape of the region does not change significantly from Figure 2. Thus, the HDR of LAEs found at $z = 3.1$ in this field is considered to be a robust structure. In the following analysis, we use the SN7.5 sample consists of 283 LAEs.

3.2. Absorbers

Besides the strong Ly α emitters, we also searched for absorbers, namely, narrowband-deficit objects in the field. In Figure 4 we show a color-magnitude diagram for the BV -selected objects. Among the sources with $BV < 26.2$ mag ($S/N > 8$), we detected 49 NB497-deficit objects that satisfy $BV - \text{NB497} < -0.7$, $B_{AB} - \text{NB497} < -0.6$, and the condition that the $BV - \text{NB497}$ color can be determined at significance level higher than 3.5σ . The first criterion corresponds to the equivalent width limit of -36 \AA , and the second ensures

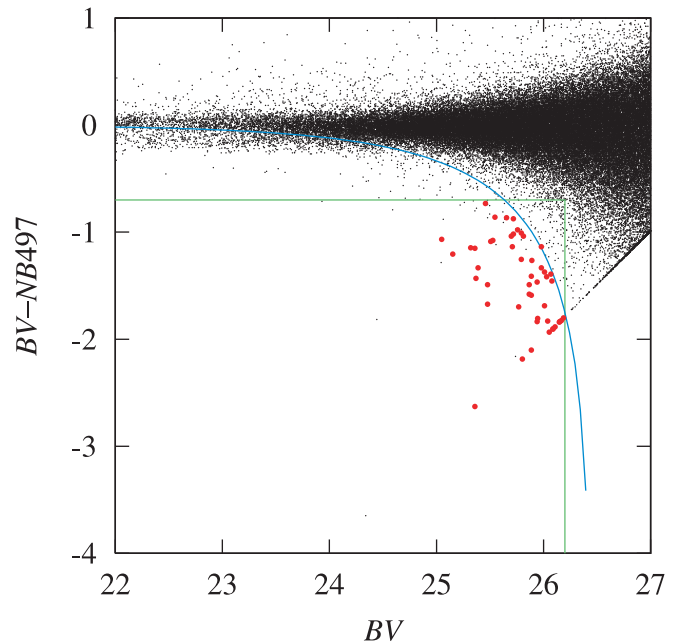


FIG. 4.—Color-magnitude plot for the BV selected objects. The blue line indicates the 3.5σ confidence level for NB497 deficit. The horizontal green line shows $BV - \text{NB497} = -0.7$, which corresponds to the equivalent width of -36 \AA . The vertical green line indicates $BV = 26.2$ ($S/N = 8$) after correction for the Galactic extinction (see text). The Ly α absorber candidates at $z = 3.1$ that satisfy the criteria presented in the text are indicated by red filled circles.

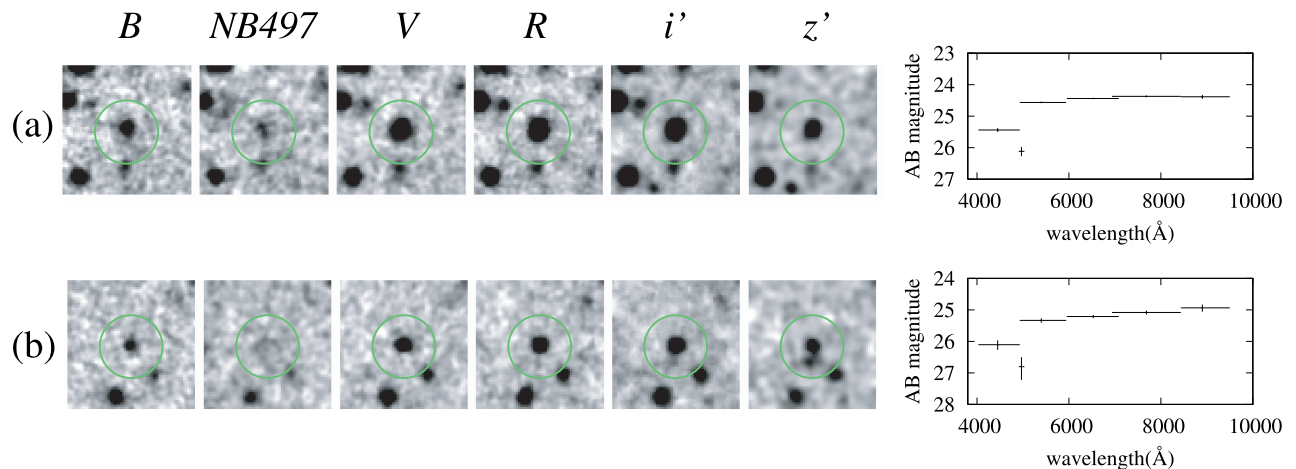


FIG. 5.—Examples of Ly α absorbers, i.e., narrowband deficit objects. Box size is 20''. The object in (a), SSA22a-C19, is a spectroscopically confirmed LBG at $z = 3.1$.

that the feature is an absorption line and not a continuum break. Many of these sources must be Ly α absorption galaxies at $z = 3.1$ or background objects that have strong absorption-line systems at $z = 3.1$ (hereafter referred to as Ly α absorbers). Only 3.5 nonabsorption objects ($BV - NB497 \approx 0$) are expected to be contaminating the present absorber sample because of photometric errors. The images and the low-dispersion spectra obtained from the broad- and narrowband magnitude of the two strong absorbers are shown as examples in Figures 5a and 5b. The object in Figure 5a corresponds to a spectroscopically confirmed LBG at $z = 3.103$ (Steidel et al. 1998). In Figure 2, we show the distribution of the Ly α absorbers with filled red

circles. It is remarkable that their distribution is very similar to that of the LAEs. Out of the 49 absorbers, 41 are in the HDR, with an area of only 40% of the entire field. This strongly suggests that the HDR of the LAEs is indeed a real large-scale structure at $z = 3.1$ and that these absorbers are associated with it.

3.3. Extended Emitters

During the course of eye inspection of our narrowband excess image made by subtracting the BV image from the NB497 one (referred to as the $NB497 - BV$ image), we found a number of extended sources in addition to the two gigantic LABs

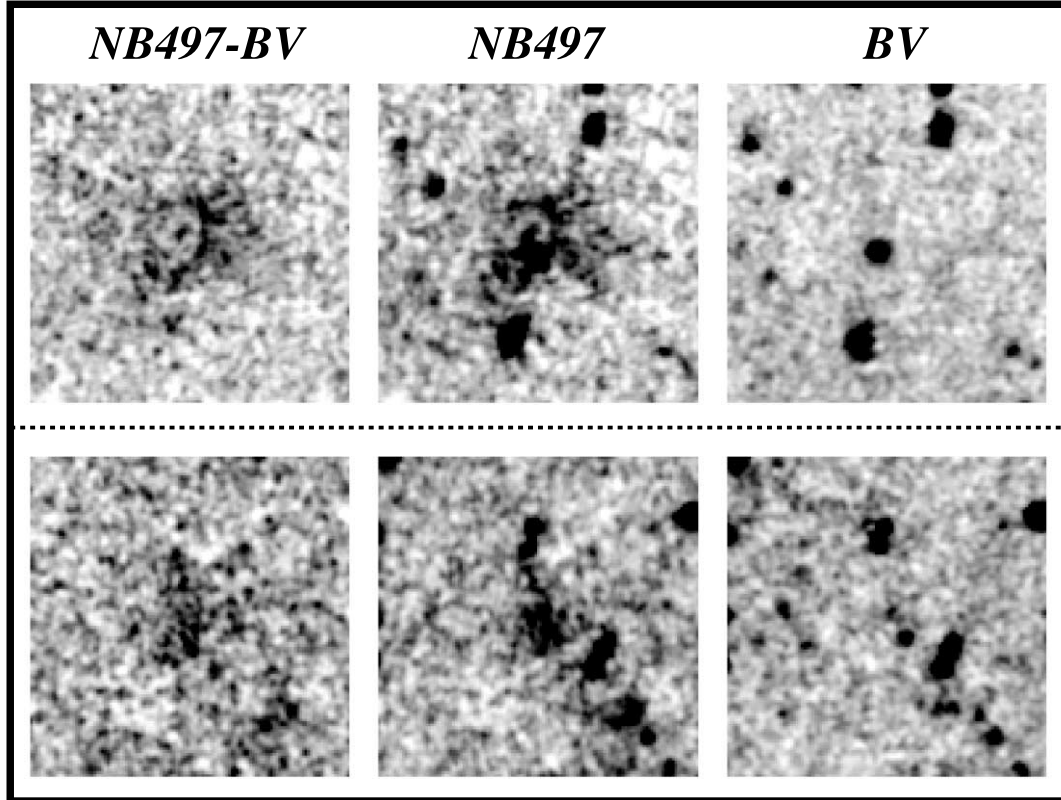


FIG. 6.—NB497 – BV , NB497, and BV images for two typical extended Ly α emitters. Box size is 24''.

discovered by Steidel et al. Their NB497 excess fluxes and angular sizes are smaller than the two LABs. We call them extended Ly α emitters, or simply extended emitters. We selected the extended emitters using SExtractor version 2.2.2 (Bertin & Arnouts 1996) in a way similar to that adopted in Matsuda et al. (2004), applying slightly fainter criteria as follows. First, we detected the object on the NB497 – BV image smoothed with a Gaussian kernel of 1" FWHM, requiring 450 contiguous pixels (18 arcsec 2) above the threshold of 4.5 counts pixel $^{-1}$, which corresponds to 28.4 mag arcsec $^{-2}$ (1.6×10^{-18} ergs s $^{-1}$ cm $^{-2}$ arcsec $^{-2}$), or to the 1.4σ arcsec $^{-2}$ of the sky fluctuation of the presmoothed NB497 – BV image. Then we applied the color criterion of $BV - NB497 > 0.7$, where the color is measured in the isophotal aperture defined in the source detection. $BV - NB497 > 0.7$ corresponds to an observed EW of 80 Å. Moreover, we required our sample to have a significances of 6σ or more of the sky fluctuation in each isophotal aperture on the NB497 – BV image. In this way, we detected 74 extended emitters that satisfy these criteria and are not associated with the gigantic LABs (Steidel et al. 2000). The flux limit in the present selection is 24.7 mag (4.7×10^{-17} ergs s $^{-1}$ cm $^{-2}$) on the NB497 – BV image. We examined the reliability of the 74 extended emitters by carrying out the same detection and selection procedures on the reversed images constructed by multiplying the original images by -1 , as performed in Matsuda et al. (2004). Any false objects are revealed in this procedure. Among the 74 extended emitters, 36 are already included in a sample of the 424 Ly α emitters with the lower flux and EW limits. Thus, 38 new extended emitters are found using this selection procedure. Among the 35 LABs found and discussed in Matsuda et al. (2004), 30 are included in the present extended emitter sample, while two objects are the gigantic LABs (Steidel et al. 2000) and the remaining three have smaller isophotal areas than the threshold adopted in this paper.

Two newly discovered typical examples are shown in Figure 6. The spatial distribution of the 74 extended emitters is also shown in Figure 2 (*open blue squares*). Again, the overall sky distribution of the extended emitters is very similar to that of the LAEs, as well as the sky distribution of the Ly α absorbers. Of the 74 extended emitters, 56 are in the HDR of the LAEs, and the others, except for a few extended emitters, lie on the borders of the HDR. It is very important that the three kinds of Ly α objects selected in different manners have very similar sky distributions. Again, this strongly supports the reality of the large-scale structure that we have found at $z = 3.1$.

4. DISCUSSION

We found that the high-density region of Ly α emitters at $z = 3.1$ in the SSA22a field discovered by Steidel et al. extends more than 60 Mpc in comoving length over our survey field of $32' \times 24'$. It is also remarkable that the Ly α absorbers, as well as the extended Ly α emitters, are also preferentially distributed in the high-density region of the strong Ly α emitters, indicating that the region is the place where galaxy formation frequently occurs. It is interesting to consider the significance of the overdensity of this newly found large-scale structure in the context of the CDM structure formation scenario. We first compare the surface number density of the LAEs at $z = 3.1$ in the SSA22 HDR with those measured in the SXDS-GT field. Since they are observed with the same narrowband filter, surface densities can be directly translated to the spatial densities averaged over the volume sampled by the filter. Because the

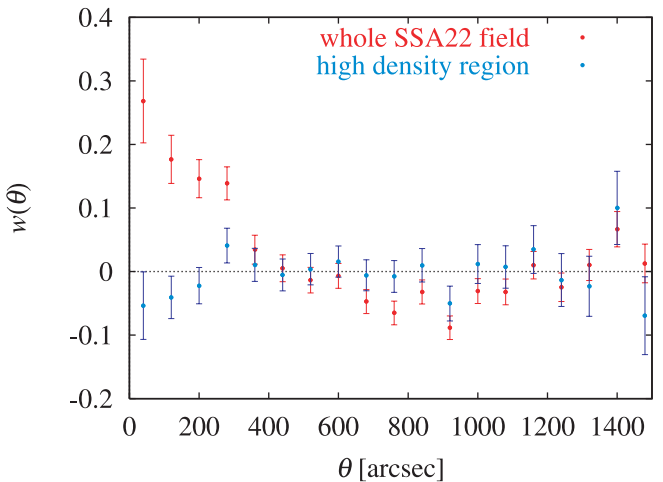


FIG. 7.—Angular two-point correlations of the strong Ly α emitters. The blue and red circles show emitters belonging to the high-density region and to our SSA22 entire field, respectively.

SXDF-GT narrowband image is shallower than that of SSA22, we only compare the numbers of the detected objects with $NB497 < 25.3$ (Table 1). Assuming that the SXDS-GT field represents a general “blank field,” where the number density of the LAEs is close to the universal average, we may evaluate the density enhancement of the SSA22 HDR. We obtained $\delta_{\text{em}}(\text{SSA22 HDR}) = [\rho_{\text{em}}(\text{SSA22 HDR}) - \rho_{\text{em}}(\text{SXDF})]/\rho_{\text{em}}(\text{SXDF}) = 1.8 \pm 0.5$. On the other hand, a 1σ mass fluctuation, $\sigma_M = 0.14$, is expected from the linear growth theory of CDM fluctuations for the equivalent spherical volume, $9 \times 10^4 h_{70}^{-3}$ Mpc 3 , with the normalization $\sigma_8 = 1.0$. It is found that $\delta_{\text{em}}(\text{SSA22 HDR})$ is 13 times larger than σ_M . If we take the LAE bias parameter to mass, $\sigma_{\text{LAE}}/\sigma_M$, at $z = 3.1$ to be ~ 4 , as inferred for LBGs at similar redshift (Steidel et al. 1998; Adelberger et al. 1998), there is only 3σ probability of finding such a large-scale high-density region. SSA22 HDR must be a very rare high-density peak in the universe.

It is also interesting to investigate internal structure of the high-density region. Steidel et al. (2000) reported that there is no significant clustering of their emitters inside the SSA22a area. In Figure 7, we show the angular two-point correlation function $w(\theta)$ of the LAEs that belong to the HDR (*blue circles*), as well as that of the entire Prime-Cam field (*red circles*). The LAEs in our sample inside the HDR show no positive correlation, while an apparent correlation appears on small scales of less than $\sim 5'$ if we calculate $w(\theta)$ over the entire field. The LAEs inside the HDR do not seem to be clustered.

We found that nine extended emitters are the LBGs discovered by Steidel et al. (1998). We then investigated diffuse Ly α emission, i.e., the Ly α halo, associated with the known LBGs in our field. We found that 24 spectroscopically confirmed LBGs from the list by Steidel et al. (2003) with redshifts between 3.061 and 3.125, namely, in the Ly α window of NB497, lie in the field. Only two of these are selected with our criteria as LAEs. After removing two other LBGs associated with the two gigantic LABs (Steidel et al. 2000) from the sample, we made an average composite NB497 – BV image of the 22 LBGs as shown in Figure 8a. The average radial profile and the distribution of the flux in “ring aperture” of $r = 2'' - 4''$ of the 22 LBGs are also shown in Figures 8b and 8c. It is remarkable that these LBGs, on average, have a Ly α emission-line halo that extends to $\approx 5''$ in radius, corresponding, on average, to

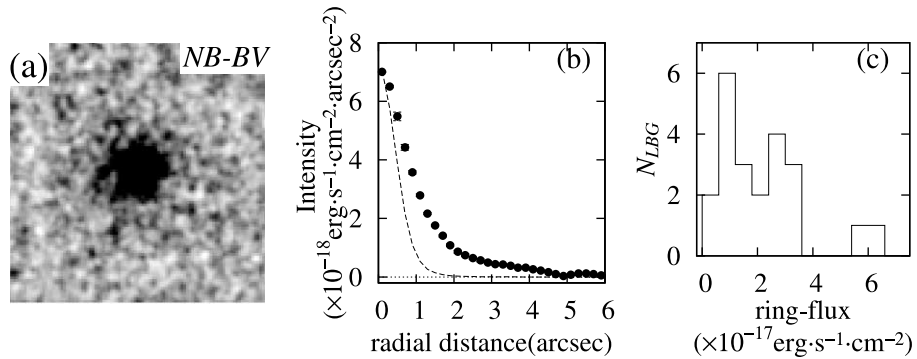


FIG. 8.—(a) Composite NB497 – BV image of the 22 LBGs. Box size is $20''$. (b) Radial profile of the composite image. The dotted line shows the average profile of 16 pointlike sources on our BV image. (c) Distribution of flux in “ring aperture” with $2''$ – $4''$ radius for the 22 LBGs on the NB497 – BV image. The 1σ sky fluctuation in the ring aperture is $9.4 \times 10^{-18} \text{ ergs}^{-1} \text{ cm}^{-2}$.

~ 40 kpc in proper length. It is noteworthy that 13 LBGs not detected as extended emitters also show Ly α halos on their composite NB497-BV image. This means that almost all LBGs in the Ly α window of NB497 have Ly α halos in the present field.

Finally, we would like to note that this large scale-structure can be only a part of a further huge structure, since the beltlike structure of the high-density region reaches to the edges of our observed field of view. It would be necessary to carry out a further extended survey—both spatially and along redshift—to reveal the true three-dimensional extension of the density peak.

We thank the staff of the Subaru Telescope for their assistance with our observations. This work is partially supported by grants-in-aid for scientific research from the Ministry of Education, Culture, Sports, Science, and Technology (14540234). Based in part on data collected at Subaru Telescope and obtained from data archive at Astronomical Data Analysis Center, which are operated by the National Astronomical Observatory of Japan. The Image Reduction and Analysis Facility (IRAF) used in this paper is distributed by the National Optical Astronomy Observatory, which is operated by the Association of Universities for Research in Astronomy, Inc., under cooperative agreement with the National Science Foundation.

REFERENCES

- Adelberger, K. L., Steidel, C. C., Giavalisco, M., Dickinson, M., Pettini, M., & Kellogg, M. 1998, ApJ, 505, 18
- Bertin, E., & Arnouts, S. 1996, A&AS, 117, 393
- Cen, R., & Ostriker, J. P. 2000, ApJ, 538, 83
- Chapman, S. C., Lewis, G. F., Scott, D., Richards, E., Borys, C., Steidel, C. C., Adelberger, K. L., & Shapley, A. E. 2001, ApJ, 548, L17
- Governato, F., Baugh, C. M., Frenk, C. S., Cole, S., Lacey, C. G., Quinn, T., & Stadel, J. 1998, Nature, 392, 359
- Hammer, F., et al. 1997, ApJ, 481, 49
- Kauffmann, G., Colberg, J. M., Diaferio, A., & White, S. D. M. 1999, MNRAS, 307, 529
- Madau, P. 1995, ApJ, 441, 18
- Matsuda, Y., et al. 2004, AJ, 128, 569
- Miyazaki, S., et al. 2002, PASJ, 54, 833
- Ohyama, Y., et al. 2003, ApJ, 591, L9
- Ouchi, M., et al. 2001, ApJ, 558, L83
- Ouchi, M., et al. 2003, ApJ, 582, 60
- Shimasaku, K., et al. 2003, ApJ, 586, L111
- Steidel, C. C., Adelberger, K. L., Dickinson, M., Giavalisco, M., Pettini, M., & Kellogg, M. 1998, ApJ, 492, 428
- Steidel, C. C., Adelberger, K. L., Shapley, A. E., Pettini, M., Dickinson, M., & Giavalisco, M. 2000, ApJ, 532, 170
- . 2003, ApJ, 592, 728
- Sullivan, M., Treyer, M. A., Ellis, R. S., Bridges, T. J., Milliard, B., & Donas, J. 2000, MNRAS, 312, 442
- Treyer, M. A., Ellis, R. S., Milliard, B., Donas, J., & Bridges, T. J. 1998, MNRAS, 300, 303
- Watson, M. G., & Sekiguchi, K. 2001, Two Years of Science with Chandra, Abstracts from the Symposium, 94
- Yagi, M., Kashikawa, N., Sekiguchi, M., Doi, M., Yasuda, N., Shimasaku, K., & Okamura, S. 2002, AJ, 123, 66